Available online at www.sciencedirect.com
SCIENCE DIRECT®
ELSEVIER
Nuclear Instruments and Methods in Physics Research B 202 (2003) 300–304
NIM B
Beam Interactions with Materials & Atoms
www.elsevier.com/locate/nimb

PIC-MC simulation of an RF capacitively coupled Ar/H_2 discharge

E. Neyts, M. Yan, A. Bogaerts *, R. Gijbels

Department of Chemistry, University of Antwerp, Universiteitsplein 1, B-2610 Antwerp, Belgium

Abstract

A 1D3v self-consistent particle-in-cell/Monte Carlo simulation is used to investigate the role of small amounts of hydrogen added to an RF capacitively coupled argon discharge at low pressure. The addition of H_2 has an important effect on the discharge behaviour, especially on the electron density, the density of the various ions, and the electron energy probability function. These effects can be explained in terms of the collision processes taking place in the discharge. The simulations were carried out in the pressure range 100–250 mTorr, at a voltage of 300 V, and a driving frequency of 13.56 MHz. The partial hydrogen pressure was in the range 0–10%.
© 2002 Elsevier Science B.V. All rights reserved.

PACS: 52.65.Pp; 52.65.Rr
Keywords: Argon/hydrogen RF discharge; Plasma simulation; Particle-in-cell/Monte Carlo

1. Introduction

Argon/hydrogen discharges are frequently used for surface cleaning purposes [1] and sputter–deposition processes [2], and they are also a topic of interest for analytical applications [3,4]. In [10], an overview of the possible reactions in an Ar/H_2 discharge is given. Experimentally, Mason et al. [11] studied the anomalous loss of ionisation in an Ar/H_2 plasma by fast flow glow discharge mass spectrometry. Ar/H_2 discharges were also investigated by Meulenbroeks et al. [12] in a plasma jet. Electron energy distribution functions (EEDFs) have been measured for Ar/H_2 CCDs by Müller [13].

Particle-in-cell (PIC) and PIC/Monte Carlo (PIC-MC) simulations have been used extensively to study the fundamental processes in capacitively coupled discharges (CCDs), e.g. [5–9], but to the authors' knowledge, no attempt has been made so far to model an Ar/H_2 discharge by PIC-MC simulations. In this paper, we study the influence of small amounts of H_2 in an Ar discharge for different conditions with a PIC-MC model.

2. Description of the model

The model used in this work is a classical PIC-MC code and more information about the basic ideas of both PIC and PIC-MC can be found in

* Corresponding author. Tel.: +32-3-820-2377; fax: +32-3-820-2376.
E-mail address: bogaerts@uia.ua.ac.be (A. Bogaerts).

0168-583X/02/$ - see front matter © 2002 Elsevier Science B.V. All rights reserved.
doi:10.1016/S0168-583X(02)01873-6

[6,14–16]. It was developed earlier for argon by Yan. The MC part of this code is based on the model of Vahedi and Surendra [6]. In the present work, this model is extended to an Ar/H_2 discharge. The species taken into account in our model are electrons, Ar^+, ArH^+, H_2^+ and H_3^+ ions, Ar atoms and H_2 molecules. H atoms and H^+ ions are not considered, because of the very low dissociation degree of H_2 [25] and the very low H^+ density. Excited atoms are not followed either; excitation reactions serve only as an energy loss for the electrons. Neutrals are considered as a continuum, and are not followed as particles. It is assumed that they have a Maxwellian velocity distribution at a gas temperature $T = 0.026$ eV (300 K). The hydrogen concentration – expressed as a partial pressure – in the discharge is fixed at a predefined value. Furthermore, the walls are assumed to be perfectly recombining. The choice of reactions is based on [10]. The reactions taken into account in the model are given in Table 1.

3. Results and discussion

All calculations are performed for a symmetric discharge cell with an interelectrode distance $d = 2.5$ cm and with a parallel plate geometry. Typical calculation results will be presented for a discharge voltage of 300 V, and pressures of 100 and 250 mTorr. The hydrogen concentration is varied between 0% and 10%.

3.1. The electron energy probability function

The electron energy probability function (EEPF) is defined as

$$f(\varepsilon) = F(\varepsilon)\varepsilon^{-1/2},$$

where $F(\varepsilon)$ is the EEDF and ε is the electron energy. The EEPF is normalised such that the integral over the energy equals 1.

In Fig. 1, the EEPFs are shown for a pure argon discharge, and for the Ar/H_2 mixture, at ratios

Table 1
Overview of the reactions taken into account in the model, as well as the references where the cross sections were obtained from

Reaction number	Reaction	Reaction type	Ref.
1	$e + Ar \rightarrow e + Ar$	Elastic scattering	[17]
2	$e + Ar \rightarrow e + Ar^*$	Excitation	[17]
3	$e + Ar \rightarrow 2e + Ar^+$	Ionisation	[17]
4	$e + H_2 \rightarrow e + H_2$	Elastic scattering	[21]
5	$e + H_2 \rightarrow e + H_2^*$	Vibrational excitation	[21]
6	$e + H_2 \rightarrow e + H_2^*$	Singlet excitation	[21]
7	$e + H_2 \rightarrow 2e + H_2^+$	Ionisation	[21]
8	$e + H_2 \rightarrow e + H_2^* \rightarrow e + 2H$	Triplet excitation, followed by dissociation	[21]
9	$e + H_2^+ \rightarrow 2H$	Recombination	[18]
10	$e + H_3^+ \rightarrow H + H_2$	Recombination	[18]
11	$e + ArH^+ \rightarrow H + Ar$	Recombination	[18]
12	$Ar^+ + Ar \rightarrow Ar^+ + Ar$	Elastic scattering	[6]
13	$Ar^+ + Ar \rightarrow Ar + Ar^+$	Symmetric charge transfer	[6]
14	$Ar^+ + H_2 \rightarrow Ar + H_2^+$	Charge transfer	[19]
15	$Ar^+ + H_2 \rightarrow ArH^+ + H$	H-atom transfer	[19]
16	$H_2^+ + H_2 \rightarrow H_2 + H_2^+$	Symmetric charge transfer	[20,22]
17	$H_2^+ + H_2 \rightarrow H_3^+ + H$	Proton transfer	[20,22]
18	$H_2^+ + Ar \rightarrow ArH^+ + H$	Proton transfer	[19,23]
19	$H_2^+ + Ar \rightarrow H_2 + Ar^+$	Charge transfer	[19,23]
20	$H_3^+ + Ar \rightarrow H_3^+ + Ar$	Elastic scattering	[19,23,24]
21	$H_3^+ + Ar \rightarrow ArH^+ + H_2$	Proton transfer	[19,23,24]
22	$H_3^+ + Ar \rightarrow (H^+) + H_2 + Ar$	Collision-induced dissociation	[19,23,24]
23	$ArH^+ + Ar \rightarrow ArH^+ + Ar$	Elastic scattering	[23]
24	$ArH^+ + H_2 \rightarrow ArH^+ + H_2$	Elastic scattering	[23]
25	$ArH^+ + H_2 \rightarrow H_3^+ + Ar$	Proton transfer	[23]

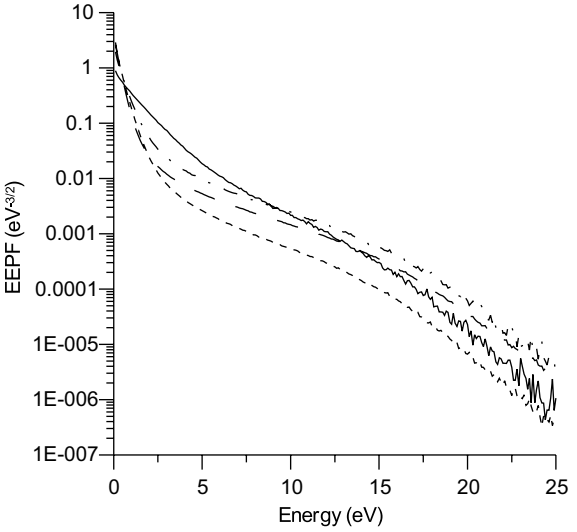

Fig. 1. Calculated EEPF for argon (solid line), and admixtures of 1% H_2 (small dashed lines), 5% H_2 (wide dashed lines) and 10% H_2 (alternating small and wide dashed lines), as a function of the electron energy, at 300 V and 100 mTorr.

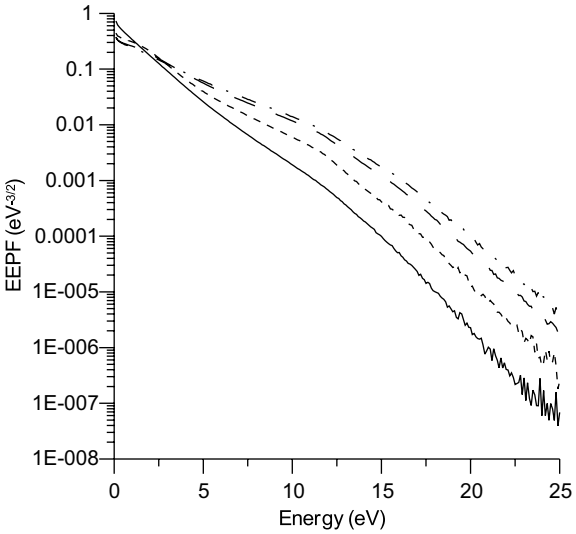

Fig. 2. Calculated EEPF for argon, and admixtures of 1%, 5% and 10% H_2, as a function of the electron energy, at 300 V and 250 mTorr. The same symbols are used as in Fig. 1.

99/1, 95/5 and 90/10, each at 100 mTorr and 300 V. In all four cases, a bi-Maxwellian energy distribution is formed, with a high-energy group (due to stochastic electron heating) and a larger low energy group (representing bulk electrons). Relative to the pure argon discharge, the EEPFs of the mixtures show an increase in the fraction of electrons with energies below 1 eV, and a decrease in the fraction of electrons with energies above 1 eV. This is due to the very low excitation threshold of vibrational excitation of H_2 (reaction 5 in Table 1), at 0.54 eV, serving as an effective energy loss for the electrons above about 1 eV in the Ar/H_2 discharges. Above 10–15 eV, the fraction of electrons becomes again higher in the Ar/H_2 mixture in the ratios 95/5 and 90/10.

At higher pressure (250 mTorr), the opposite effect takes place as can be seen in Fig. 2, i.e. a lower fraction of low energy electrons relative to the pure argon case, and a higher fraction of high energy electrons. Furthermore, a Druyvenstein-like distribution is now formed. Indeed, at this pressure, the discharge is collision-dominated, and the heating of the electrons occurs primarily in the bulk of the discharge. The inversion both at low and high energy is due to the so-called loss of ionisation. This loss of ionisation is attributed in [12] to a combination of a H-atom transfer reaction (reaction 15 in Table 1), followed by efficient recombination (reaction 11) while in [11] this loss of ionisation is assumed to be due to a decrease in the Ar-metastable density, which would be the precursors for most ions. However, in our simulation, reaction 11 is found to be negligible, and Ar-metastables are not included. Reaction 15, however, is the main mechanism of ArH^+ formation and Ar^+ loss. These ions constitute the main positive ion density, together with H_3^+, which is also created in an ion–molecule reaction. Therefore, ionisation itself becomes less critical for plasma maintenance. Also, this loss of ionisation is partly responsible for the lower electron density in Ar/H_2 discharges under these conditions (see below).

3.2. Density profiles

In Fig. 3, the time-averaged electron densities are shown for 300 V at 100 mTorr, for pure argon, and for 1%, 5% and 10% H_2 added. As can be seen, the electron density increases at low H_2

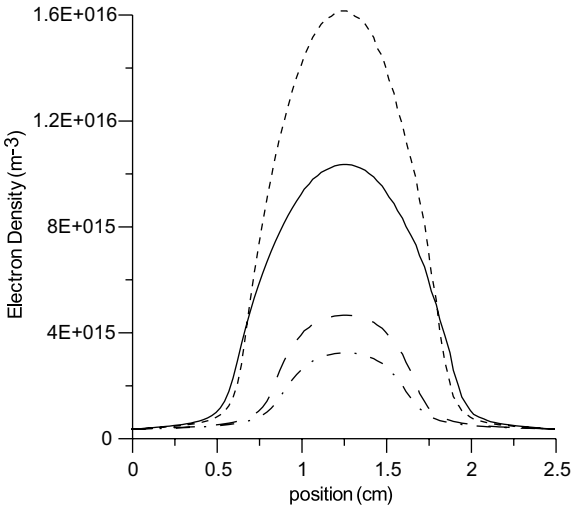

Fig. 3. Calculated time-averaged electron density for argon, and admixtures of 1%, 5% and 10% H_2, as a function of the axial position in the discharge, at 300 V and 100 mTorr. The same symbols are used as in Fig. 1.

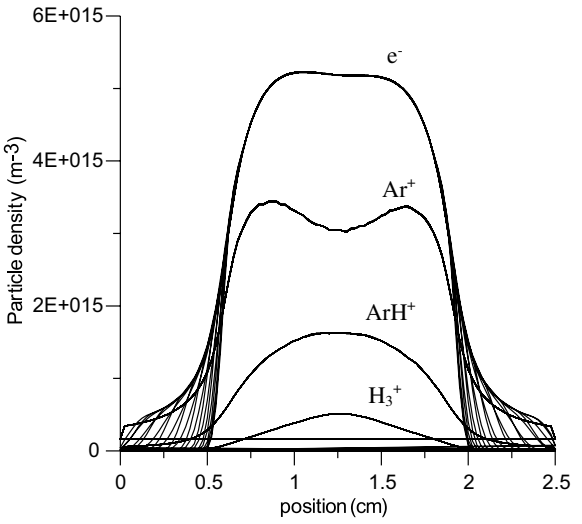

Fig. 4. Calculated particle densities for the 99/1 ratio Ar/H_2 discharge as a function of the axial position in the discharge, at 300 V and 250 mTorr. The multiple lines for the electron density represent the oscillation of the electron cloud due to the back and forth moving sheaths. The H_2^+ density is not shown, because it is three orders of magnitude lower than the Ar^+ ion density.

content, relative to the pure argon discharge, and decreases for higher H_2 content. This result can be explained by the EEPF (Fig. 1). Indeed, the fraction of very low energy electrons is significantly higher in the 1% H_2 case than in any other case, resulting in a large fraction of electrons not capable of surpassing the ambipolar potential to get lost at the walls, resulting in a higher electron density. Moreover, the fraction high energy electrons (from about 2.5 eV) is significantly lower than in any other case, resulting in reduced loss at the walls.

At higher pressure (250 mTorr) the situation is reversed as can be seen in Fig. 2. This figure shows that the pure argon discharge has the highest fraction of low energy electrons, and the lowest fraction of high energy electrons. With increasing H_2 partial pressure, the fraction low energy electrons decreases, and the fraction high energy electrons increases, resulting in the decreasing electron density at increasing partial H_2 pressure at 250 mTorr (not shown), due to increased electron losses at the walls.

The calculated densities of various ions are shown in Fig. 4, at 250 mTorr, 300 V, and an Ar/H_2 ratio of 99/1. The sum of the ion densities should everywhere except in the sheaths be equal to the electron density, to preserve electroneutrality. The figure shows a severe depletion of Ar^+ in the middle of the discharge, partly compensated by ArH^+ ions and H_3^+ ions. This Ar^+ ion depletion also leads to a reduced electron density due to the electroneutrality condition. The reason for this Ar^+ ion density profile is that the Ar^+ density develops near the sheaths, where most of the electron impact ionisation of Ar occurs. The rates of the reactions leading to ArH^+ (reaction 15) and H_3^+ (reaction 25), on the other hand, have reaction rates which are essentially constant throughout the discharge, so that ArH^+ and H_3^+ form a maximum density in the middle, due to diffusion, preserving electroneutrality, and preventing Ar^+ to diffuse to the middle.

4. Summary and conclusion

A capacitively coupled RF Ar/H_2 discharge was investigated with a PIC-MC model at different conditions. At low pressure (100 mTorr) and low

H_2 partial pressure (1%), the discharge shows an increase in electron density compared to a pure argon discharge, due to the low fraction of electrons capable to get lost at the walls, while the large fraction of very low energy electrons are 'captured' in the bulk of the discharge. Upon an increase in H_2 partial pressure, the electron density decreases again, due to the decrease in the fraction of low energy electrons, and an increase in the fraction of high energy electrons.

At higher pressure (250 mTorr) ion–molecule reactions prevent the electron density to increase to values higher than in pure argon due to electroneutrality, and also lead to a depletion of the Ar^+ ion density in the middle of the discharge. This depletion is partly compensated by ArH^+ and H_3^+, both having a maximum density in the middle of the discharge. At all times, H_2^+ has a density too low to play a significant role in the discharge.

Acknowledgements

E. Neyts is indebted to the Institute for the Promotion of Innovation by Science and Technology in Flanders (IWT-Flanders) for financial support. A. Bogaerts is indebted to the Flemish Fund for Scientific Research (FWO-Flanders) for financial support. M. Yan acknowledges financial support form a 'Bilateral Scientific and Technological Cooperation' project between Flanders and China (BIL 99/46). The authors also acknowledge financial support from the Federal Services for Scientific, Technical and Cultural Affairs (DWTC/SSTC) of the Prime Minister's Office through IUAP-V.

References

[1] C.V. Budtz-Jorgensen, P. Kringhoj, J. Bottiger, Surf. Coat. Technol. 116–119 (1999) 938.
[2] H. Takahashi, H. Nagata, H. Kataoka, Thin Solid Films 227 (1996) 132.
[3] V.D. Hodoroaba, V. Hoffmann, E.B.M. Steers, K. Wetzig, J. Anal. At. Spectrom. 15 (2000) 1075.
[4] V.D. Hodoroaba, V. Hoffmann, E.B.M. Steers, K. Wetzig, J. Anal. At. Spectrom. 15 (2000) 951.
[5] M. Surendra, D.B. Graves, Appl. Phys. Lett. 56 (1990) 1022.
[6] V. Vahedi, M. Surendra, Comput. Phys. Commun. 87 (1995) 179.
[7] M. Surendra, D.B. Graves, IEEE Trans. Plasma Sci. 19 (1991) 144.
[8] V. Vahedi, C.K. Birdsall, M.A. Lieberman, G. DiPeso, T.D. Rognlien, Plasma Sources Sci. Technol. 2 (1993) 272.
[9] D. Vender, R.W. Boswell, IEEE Trans. Plasma Sci. 18 (1990) 725.
[10] A. Bogaerts, R. Gijbels, J. Anal. At. Spectrom. 15 (2000) 441.
[11] R.S. Mason, P.D. Miller, I.P. Mortimer, Phys. Rev. E 55 (1997) 7462.
[12] R.F.G. Meulenbroeks, A.J. van Beek, A.J.G. van Helvoort, M.C.M. van de Sanden, D.C. Schram, Phys. Rev. E 49 (1994) 4397.
[13] M. Müller, M.Sc. Thesis, University Essen, November 1997.
[14] E. Kawamura, C.K. Birdsall, V. Vahedi, Plasma Sources Sci. Technol. 9 (2000) 413.
[15] C.K. Birdsall, A.B. Langdon, Plasma Physics via Computer Simulation, IOP Publishing Ltd., Adam Hilger Series, Bristol, 1991.
[16] V. Vahedi, G. DiPeso, C.K. Birdsall, M.A. Lieberman, T.D. Rognlien, Plasma Sources Sci. Technol. 2 (1993) 261.
[17] A.V. Phelps, Z.Lj. Petrovic, Plasma Sources Sci. Technol. 8 (1999) R21.
[18] H. Tawara, Y. Itakawa, H. Nishimura, M. Yoshino, J. Phys. Ref. Data 19 (1990) 617.
[19] A.V. Phelps, J. Phys. Ref. Data 21 (1992) 883.
[20] A.V. Phelps, J. Phys. Chem. Ref. Data 19 (1990) 653.
[21] S.J. Buckman, A.V. Phelps, J. Chem. Phys. 82 (1985) 4999.
[22] T. Tabata, T. Shirai, Atom. Data Nucl. Data Tables 76 (2000) 1.
[23] A.V. Phelps, private communication. Available from <ftp://jila.colorado.edu/collision_data>.
[24] B.L. Peko, R.L. Champion, Y. Wang, J. Chem. Phys. 104 (1996) 6149.
[25] A. Bogaerts, R. Gijbels, Spectrochim. Acta Part B 57 (2002) 1071.